

Supporting Information for

Rational design of benzodifuran-functionalized donor-acceptor covalent organic framework for photocatalytic hydrogen evolution from water

Guang-Bo Wang,[†] Fu-Cheng Zhu,[†] Qian-Qian Lin, Jing-Lan Kan, Ke-Hui Xie, Sha Li, Yan Geng^{*} and Yu-Bin Dong^{*}

College of Chemistry, Chemical Engineering and Materials Science, Collaborative Innovation Center of Functionalized Probes for Chemical Imaging in Universities of Shandong, Key Laboratory of Molecular and Nano Probes, Ministry of Education, Shandong Normal University, Jinan 250014, P. R. China.

† These authors contributed equally to this work.

Corresponding Authors: Y.-B. Dong, yubindong@sdnu.edu.cn
Y. Geng, gengyan@sdnu.edu.cn

Materials and methods

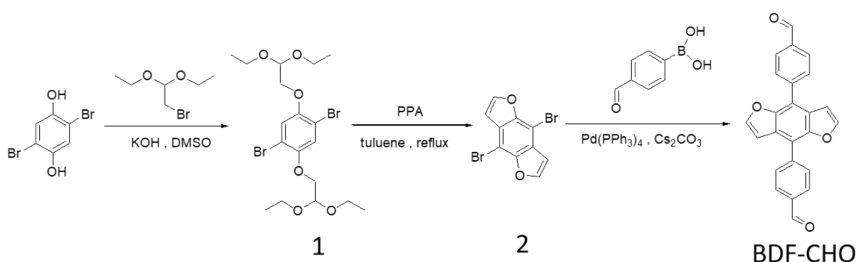
Materials. All the reagents were purchased from commercial suppliers and used without further purification unless otherwise noted. The building unit of 4,4'-(benzo[1,2-b:4,5-b']difuran-4,8-diyl)dibenzaldehyde was synthesized according to the previously reported procedures.¹

Characterizations. ^1H NMR spectra were recorded on a Bruker Avance 400 NMR spectrometer. Powder X-ray diffraction (PXRD) data were collected using a D8 ADVANCE X-ray with Cu K α radiation ($\lambda = 1.05405 \text{ \AA}$). Fourier Transform Infrared (FT-IR) spectra in the region of 800-4000 cm $^{-1}$ were obtained with a Perkin-Elmer 1600 FT-IR spectrometer. Thermogravimetric analysis (TGA) was performed on a TA Instrument Q5 analyzer with the temperature ranging from 20 to 800 °C under nitrogen and a heating rate of 10 °C/min. Scanning electron microscopy (SEM) images of the BDF-TAPT-COF material were carried out on a SUB010 scanning electron microscope with acceleration voltage of 20 kV and the transmission electron microscopy (TEM) analysis was performed on a JEOL 2100 Electron Microscope with an operating voltage of 200 kV. Solid state ^{13}C CP-MAS NMR spectrum was measured at 125.69 MHz using a 4 mm MAS NMR probe with a spinning rate of 8 kHz. Solid state UV-Vis spectra were recorded on a Cary 5000 UV-Vis spectrophotometer (Varian, USA). Time-resolved photoluminescence spectroscopy was measured by time-correlated single photon counting (Hamamatsu photonics, Quantaurus-Tau) with laser (470 nm) as the excitation light source. N₂ adsorption measurements were performed using an ASAP 2020/TriStar 3000 (Micromeritics) apparatus at 77 K, the samples were degassed under high vacuum at 120 °C for 8h before analysis.

Photoelectrochemical measurements

Cyclic voltammetry (CV) measurements were performed on a CHI 660E in a three-electrode electrochemical cell equipped with a salt bridge and a scan rate of 100 mVs $^{-1}$. The photocurrent measurements were conducted on a workstation in a standard three-electrode system in dark and light excitation at -0.14 V vs. Ag/AgCl with the photocatalyst-coated FTO as the working electrode, Pt plate as the counter electrode and Ag/AgCl as the reference electrode by directly irradiating the working electrode from the back side using a 300W Xenon lamp with AM 1.5 cut-off filter, and 2M Na₂SO₄ aqueous solution was used as the electrolyte. Electrochemical impedance spectroscopy (EIS) analysis was performed at the open circuit condition at -0.14 V vs. Ag/AgCl in the frequency range of 0.01 to 10000 Hz with an AC amplitude of 10 mV.

Synthetic procedures



Scheme S1 Synthetic routes for the building unit of 4,4'-(benzo[1,2-b:4,5-b']difuran-4,8-diyl)dibenzaldehyde (BDF-CHO).

1,4-dibromo-2,5-bis(2,2-diethoxyethoxy)benzene (1): In a 250 mL round-bottom flask, a mixture of 2,5-dibromobenzene-1,4-diol (5.0 g, 18.7 mmol), potassium

hydroxide (2.6 g, 46.7 mmol) and 150 mL DMSO was stirred at 40°C for 8h under N₂ atmosphere. Afterwards, 2-bromo-1,1-diethoxyethane (8.1g, 41mmol) was added into the mixture and heated at 80°C for another 18h. After cooling down to room temperature, the reaction mixture was poured into ice/water mixture and extracted by dichloromethane, the organic phase was combined and dried over MgSO₄ followed by the removal of the solvent in vacuo. The residue was purified with flash column chromatography on silica gel eluted with dichloromethane and subsequently recrystallized from ethanol to get white solid (4.6 g, yield of ca. 49%). ¹H NMR: δH (400 MHz, CDCl₃) 7.15(1H, s), 4.84(1H, t, J 5.2), 3.99(2H, d, J 5.2), 3.85-3.60(4H, m), 1.25(6H, t, J 7.0).

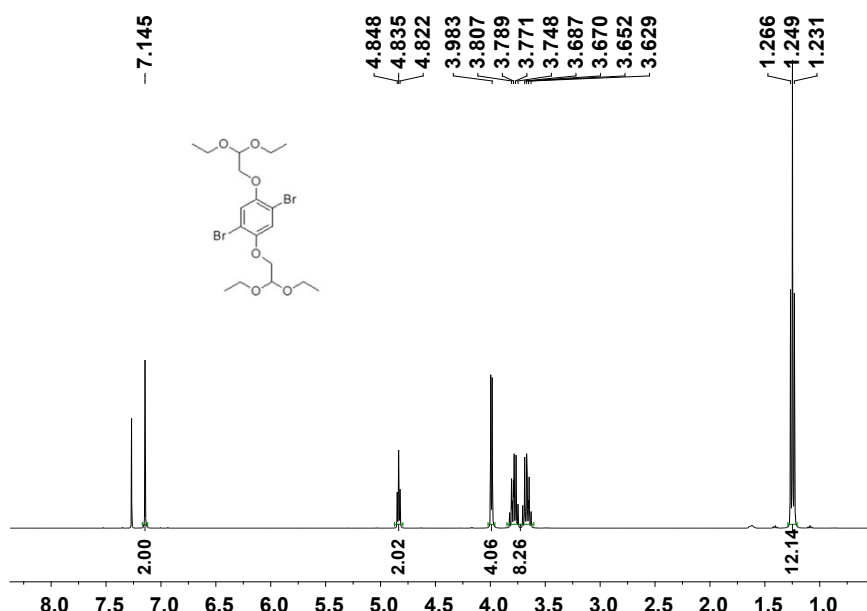


Fig. S1 ¹H NMR spectrum of compound 1.

4,8-dibromobenzo[1,2-b:4,5-b']difuran (2): A 250 mL round-bottom flask was charged with 1,4-dibromo-2,5-bis(2,2-diethoxyethoxy)benzene (1) (10.0 g, 20 mmol), polyphosphoric acid (PPA, 15 g) and toluene (100 mL), the mixture was heated at 100 °C for 5h. After cooling down to room temperature, the mixture was poured into 250 mL of 2M NaOH aqueous solution, which was extracted with dichloromethane, washed with water, dried over MgSO₄ and evaporated under vacuum. The crude product was obtained by column chromatography on silica gel eluted with petroleum ether: dichloromethane (10:1, v/v) and recrystallized from ethanol to get white solid (2.1 g, 33%). ¹H NMR: δH (400 MHz, CDCl₃) δ (ppm): 7.76 (2H, d, J 2.0), 6.98 (2H, d, J 2.0).

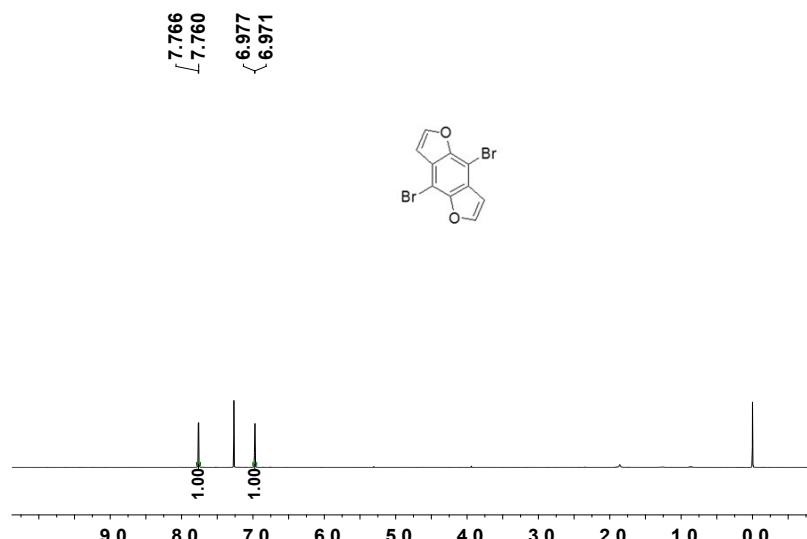


Fig. S2 ¹H NMR spectrum of compound 2.

4,4'-(benzo[1,2-b:4,5-b']difuran-4,8-diyl)dibenzaldehyde (BDF-CHO): To a stirring solution of compound 2 (3.2 g, 10 mmol), Pd(PPh₃)₄ (580 mg, 0.5 mmol) and 4-formylphenylboronic acid (3.7 g, 25 mmol) in the mixture of toluene (75 mL) and methanol (50 mL) was added 25 mL 2M CsCO₃ aqueous solution, which was degassed by N₂ bubbling in advance. After reflux for 24h under N₂, the mixture was poured into distilled water, extracted with chloroform, dried over MgSO₄ and evaporated under reduced pressure, giving the crude compound which was further purified by flash chromatography with dichloromethane as eluent and recrystallized from ethanol to afford the title product as a yellowish green powder (2.2 g, 60%). ¹H NMR: δH (400 MHz, CDCl₃) δ (ppm): 10.14 (1 H, s), 8.08 (4H, q, J8.4), 7.78 (1 H, d, J2.2), 7.06 (1H, d, J2.3).

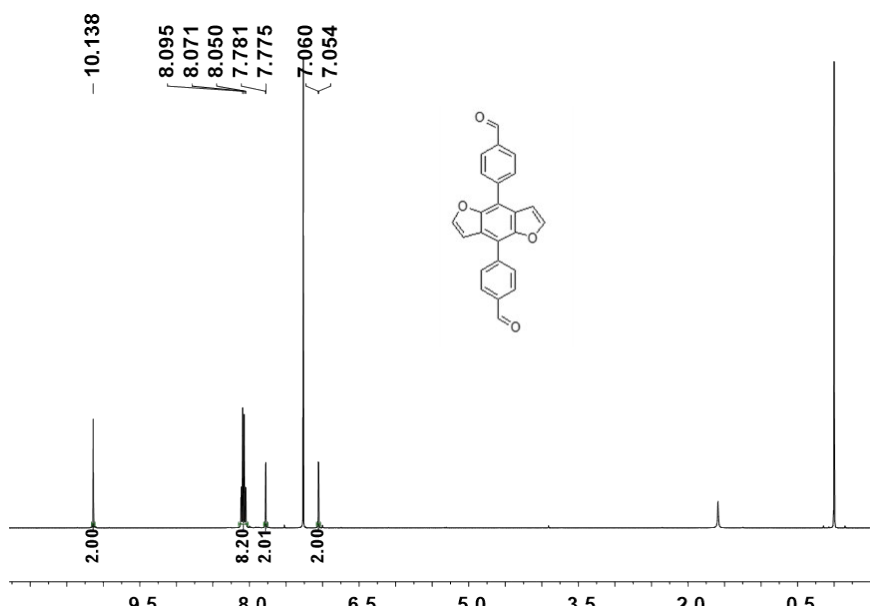


Fig. S3 ¹H NMR spectrum of BDF-CHO.

Synthesis of BDF-TAPT-COF. A Pyrex tube was charged with BDF-CHO (27.5 mg, 0.75mmol), 1,3,5-tris-(4aminophenyl)triazine (TAPT, 17.7 mg, 0.05 mmol), 0.5 mL o-dichlorobenzene and 1.5 mL n-BuOH, and then the mixture was sonicated for 10 min, followed by slow addition of 0.2 mL of 3M aqueous acetic acid. Afterwards, the tube was flash frozen at 77 K and degassed by three freeze-pump-thaw cycles, sealed under vacuum and heated at 120 °C for 3 days. After cooling down to room temperature, the tube was open and the resulting precipitate was filtered off, thoroughly washed THF, methanol and acetone until the filtrate was colorless, and Soxhlet extractions with tetrahydrofuran and dichloromethane for 24h, respectively. Finally, the resulting yellow powder was dried under vacuum at 120 °C overnight to give the **BDF-TAPT-COF** activated sample.

Details of the Photocatalysis experiments

Photocatalytic H₂ evolution experiment

The photocatalytic hydrogen evolution reactions were performed in a top-irradiation quartz vessel which was connected with an online glass closed gas circulation system (Labsolar-6A, Beijing Perfectlight). For a typical H₂ evolution experiment, the quartz vessel was charged with the activated COF powder (10 mg), 0.1 M ascorbic acid water solution (50 mL) and hexachloroplatinic acid solution as the platinum precursor. The solution was then thoroughly degassed and irradiated using a Microsolar300 Xe lamp (Beijing Perfectlight) with a cut-off filter of AM 1.5 was used as light sources. The H₂ was analyzed by gas chromatography (Fuli, 9790 II (PLF-01)) equipped with a thermal conductive detector (TCD) and a 5 Å molecular sieve column with argon as the carrier gas. After the photocatalysis experiments, the COF material was recovered by washing with water and acetone then dried under vacuum at 120 °C for multiple runs.

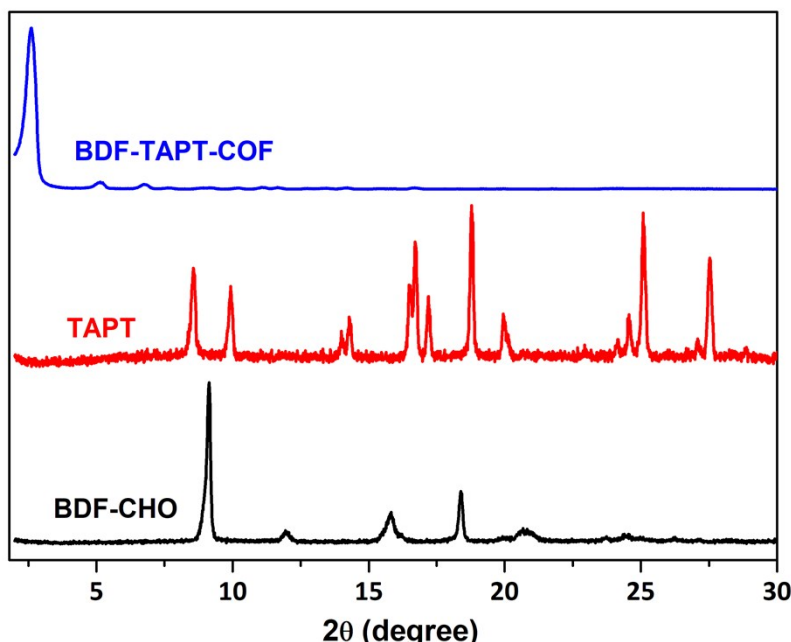


Fig. S4 PXRD patterns of BDF-CHO (black), TAPT (red) and **BDF-TAPT-COF** (blue).

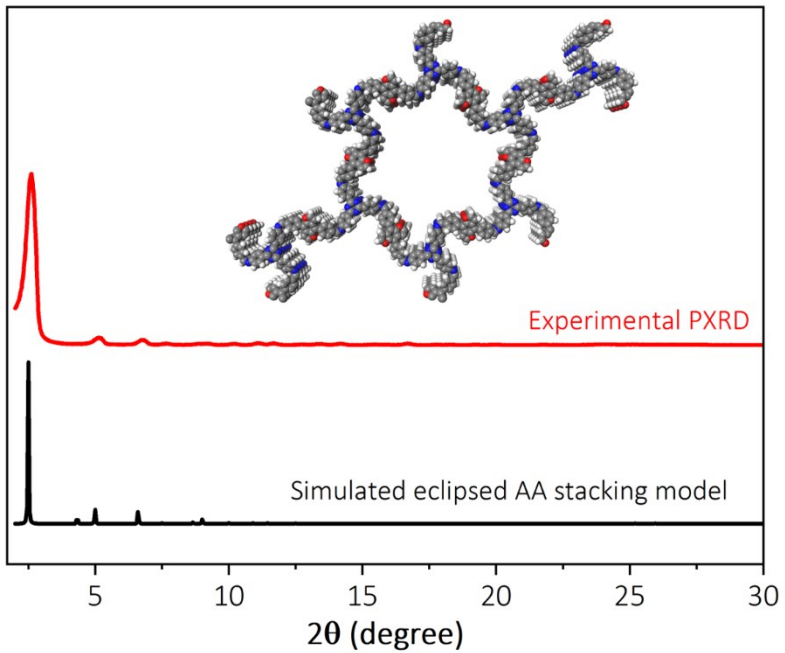


Fig. S5 Comparison of the experimental (red) and simulated AA stacking PXRD (black) patterns of **BDF-TAPT-COF** and the top view of the simulated structure of AA stacking.

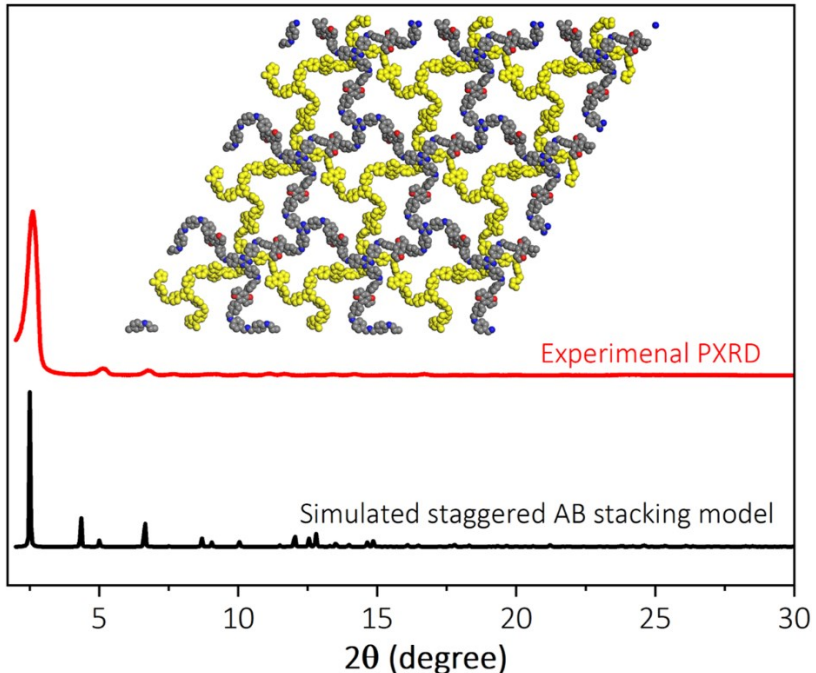


Fig. S6 Comparison of the experimental (red) and simulated AB stacking PXRD (black) patterns of **BDF-TAPT-COF** and the top view of the simulated structure of AB stacking.

Table S1 Atomistic coordinates for the AA stacking mode of **BDF-TAPT-COF** optimized using Forcite method.

Space group: <i>P</i> 3 $a = b = 40.8575 \text{ \AA}$, $c = 3.6603 \text{ \AA}$ $\alpha = \beta = 90.0^\circ$, $\gamma = 120.0^\circ$			
Pawley refinement	$R_{wp} = 10.68\%$, $R_p = 6.43\%$		
C1	0.37055	0.67775	0.91886
C2	0.4215	0.66823	0.61545
C3	0.45947	0.68195	0.52733
C4	0.48799	0.71637	0.67037
C5	0.47758	0.73884	0.86917
C6	0.43949	0.72672	0.93523
C7	0.4111	0.69083	0.81861
C8	0.55047	0.72288	0.46323
N9	0.52644	0.7341	0.54308
C10	0.51547	0.65581	0.7036
C11	0.50946	0.6194	0.70354
C12	0.53571	0.61133	0.54741
C13	0.56862	0.64054	0.38795
C14	0.57348	0.6771	0.36874
C15	0.54588	0.68468	0.51443
C16	0.55533	0.56367	0.67584
C17	0.54755	0.52664	0.69994
C18	0.51266	0.49549	0.58749
C19	0.48565	0.50484	0.46514
C20	0.49297	0.5415	0.45784
C21	0.52819	0.57235	0.55514
C22	0.46803	0.42501	0.57375
C23	0.4601	0.38918	0.45496
C24	0.48908	0.38294	0.32988
C25	0.52642	0.41279	0.35899
C26	0.53436	0.4486	0.46604
C27	0.50523	0.45588	0.55764
N28	0.49616	0.33032	0.04985
C29	0.47756	0.34807	0.11079
C30	0.53033	0.30625	0.38322
C31	0.56349	0.30526	0.44777
C32	0.5981	0.33479	0.32
C33	0.59897	0.36435	0.11865

C34	0.56549	0.3642	0.04303
C35	0.53129	0.33622	0.19066
C36	0.63324	0.33424	0.37599
O37	0.59134	0.58911	0.80716
C38	0.60534	0.56546	0.9147
C39	0.58096	0.52908	0.8606
N40	0.29567	0.65549	0.77623
N41	0.66632	0.36723	0.3671
H42	0.40036	0.64112	0.50582
H43	0.46662	0.66663	0.33435
H44	0.49958	0.76589	0.97292
H45	0.43211	0.74489	1.08659
H46	0.57714	0.74435	0.35193
H47	0.49636	0.66069	0.86198
H48	0.48443	0.59773	0.83497
H49	0.58917	0.63427	0.26367
H50	0.59777	0.69918	0.22484
H51	0.44446	0.429	0.65623
H52	0.43086	0.36686	0.43968
H53	0.55004	0.41056	0.27499
H54	0.56333	0.47091	0.45029
H55	0.44996	0.33599	-0.01395
H56	0.50338	0.28372	0.47892
H57	0.56238	0.28184	0.59973
H58	0.62497	0.38473	-0.01533
H59	0.56577	0.38415	-0.15294
H60	0.63294	0.57579	1.03511
H61	0.58569	0.50647	0.94296
O62	0.4505	0.4799	0.31717
C63	0.43587	0.5037	0.23374
C64	0.45931	0.53959	0.31398
H65	0.40792	0.49386	0.12149
H66	0.45271	0.56191	0.29139

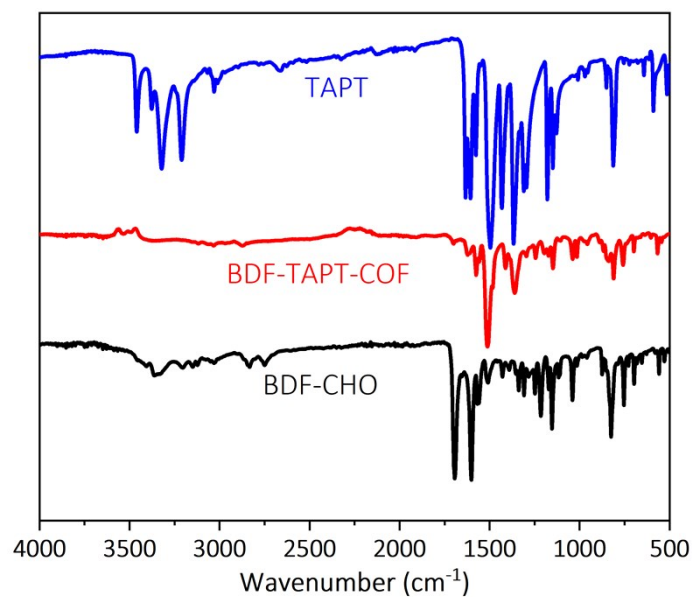


Fig. S7 FT-IR spectra of BDF-CHO (black), TAPT (blue) and **BDF-TAPT-COF** (red).

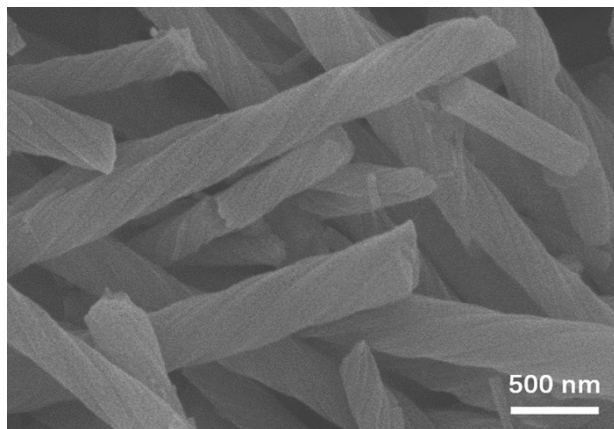


Fig. S8 Scanning electron microscopy (SEM) image of **BDF-TAPT-COF**.

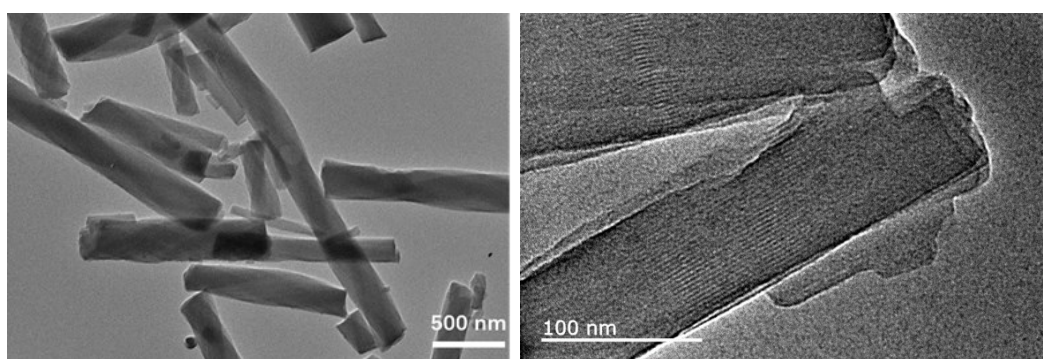


Fig. S9 Transmission electron microscopy (TEM) images of **BDF-TAPT-COF**.

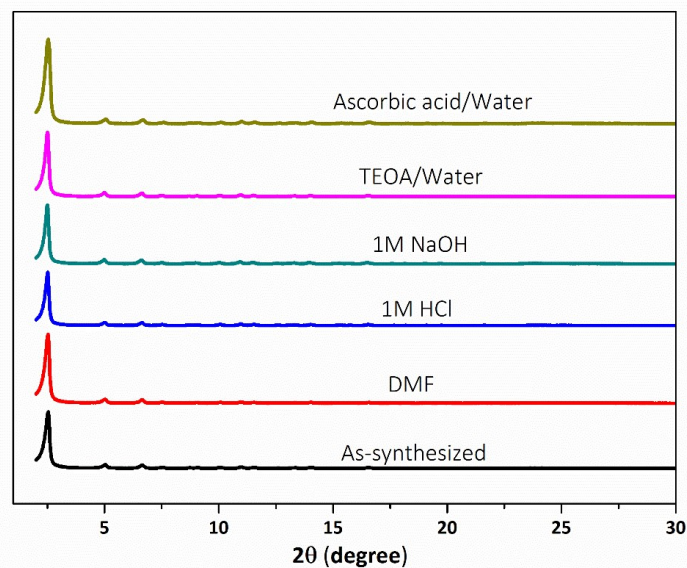


Fig. S10 Comparison of the PXRD patterns of **BDF-TAPT-COF** after immersing in different solvent for 7 days.

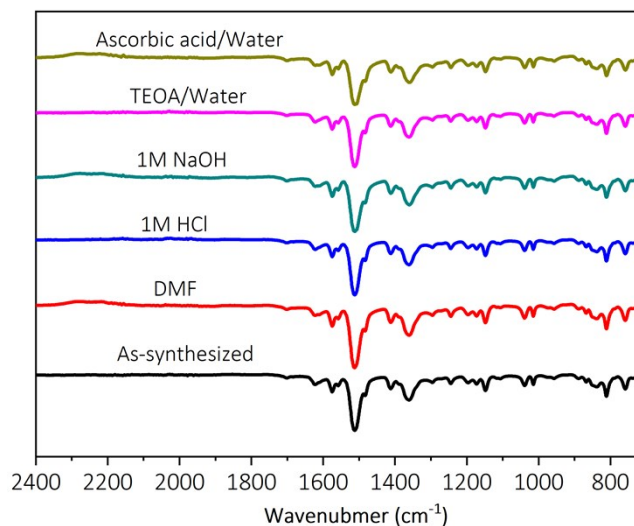


Fig. S11 Comparison of the FT-IR spectra of **BDF-TAPT-COF** after immersing in different solvents for 7 days.

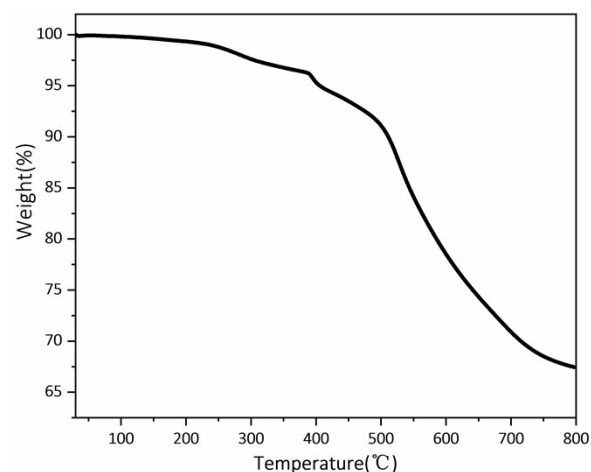


Fig. S12 Thermogravimetric analysis (TGA) curve of **BDF-TAPT-COF** measured under nitrogen flow with a heating rate 10 °C/min up to 800 °C.

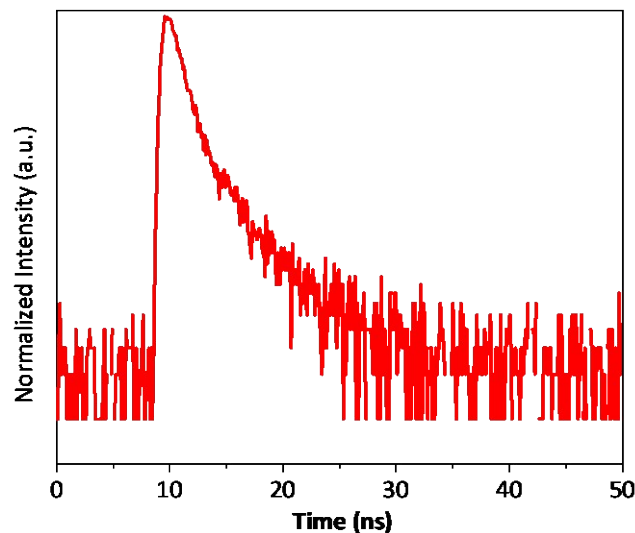


Fig. S13 Time-resolved photoluminescence spectrum of the BDF-TAPT-COF (excitation at 470 nm).

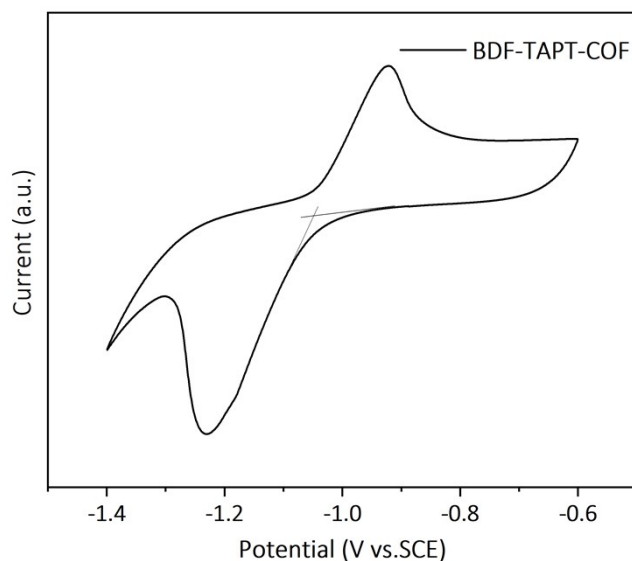


Fig. S14 Cyclic voltammetry plot of **BDF-TAPT-COF** referenced to saturated calomel (SCE) using ferrocene (F_c) as an internal standard at a scan rate of 100 mV S⁻¹.

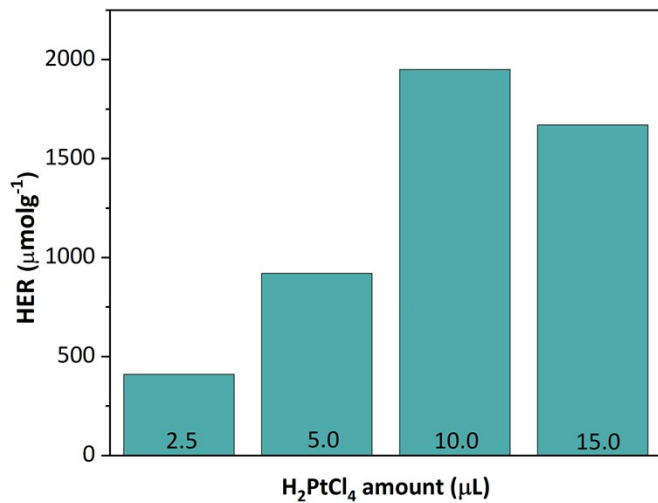


Fig. S15 Hydrogen evolution rate versus the amount of the co-catalyst (10 mg BDF-TAPT-COF, different volumes of the H₂PtCl₄ precursor in 2h under AM 1.5 irradiation).

The photocatalytic hydrogen evolution rate in 2h gradually enhanced with the increase of the amount of the Pt precursor and reached the maximum when 10 μL H₂PtCl₆ (8 wt%) was introduced, thus, the detailed photocatalytic reactions were performed under this optimized condition.

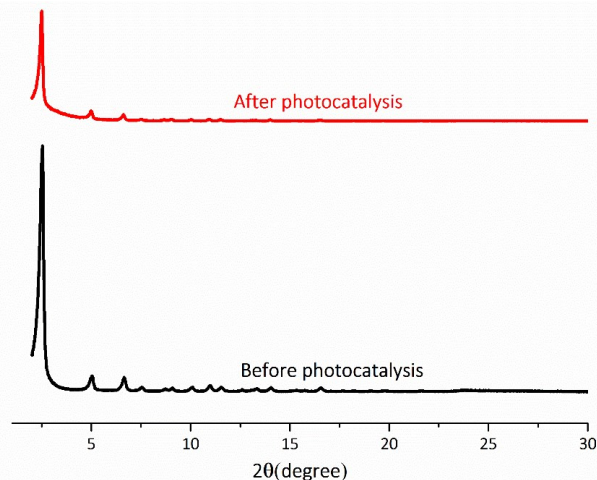


Fig. S16 PXRD patterns of **BDF-TAPT-COF** before and after photocatalytic hydrogen evolution reactions.

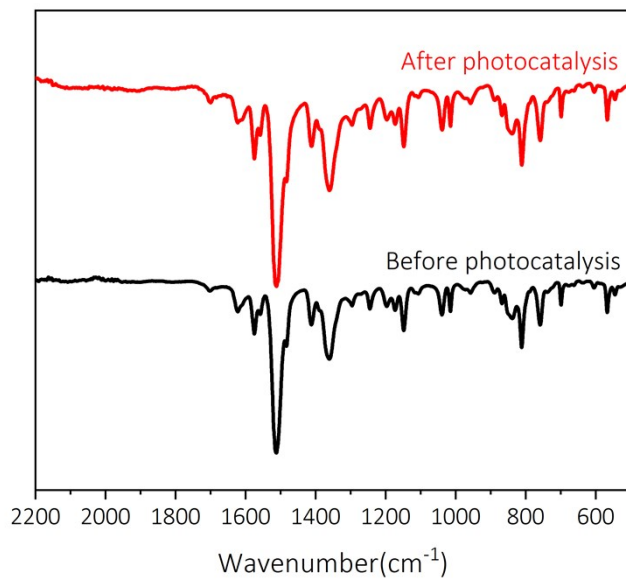


Fig. S17 FT-IR spectra of **BDF-TAPT-COF** before and after photocatalytic hydrogen evolution reactions.

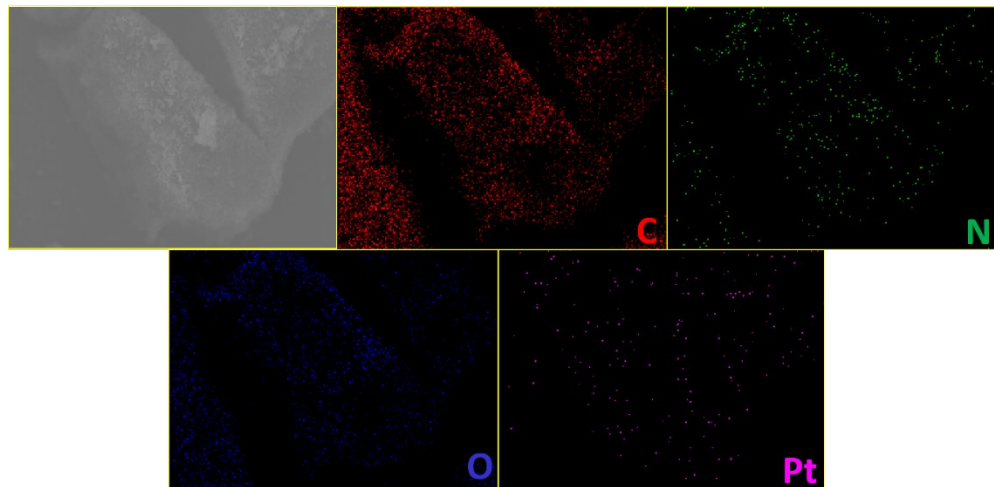


Fig. S18 SEM and EDS mapping of the **BDF-TAPT-COF** photocatalysts.

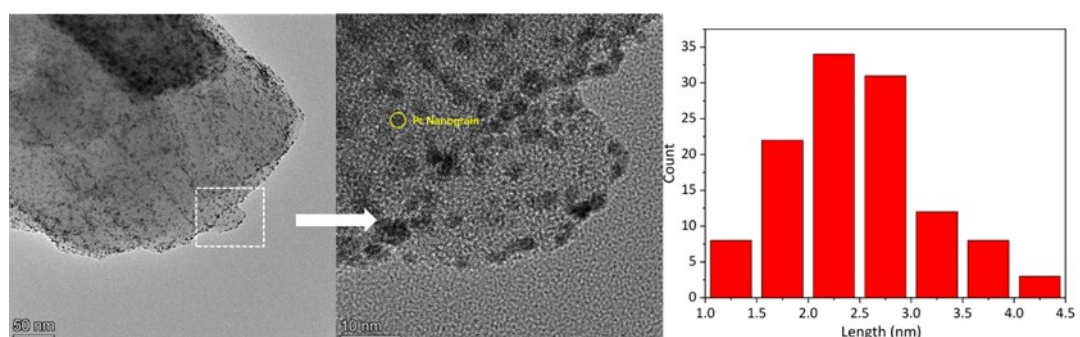


Fig. S19. TEM images of the **BDF-TAPT-COF** after photocatalysis and the corresponding diameter distribution of the Pt nanoparticles loaded on the COF material.

Table S2 The summary of the photocatalytic H₂ evolution performance under visible-light irradiation over different types of CMPs and COFs.

COFs	Band gap (eV)	Co-catalyst	Sacrificial agent	HER ($\mu\text{molg}^{-1}\text{h}^{-1}$)	AQY (%)	Ref.
g-C ₄₀ N ₃ -COF	2.36	Pt	Na ₂ S	4	-	2
TA-COF	2.82	Pt	TEOA	10	-	3
g-C ₄₀ N ₃ -COF	2.36	Pt	TEA	12	-	2
g-C ₄₀ N ₃ -COF	2.36	Pt	Na ₂ SO ₃	14	-	2
N ₀ -COF	2.6-2.7	Pt	TEOA	23	0.0017 (500 nm) ^c	4
TpPa-2-COF	2.52	Pt	Lactic acid	28	-	5
g-C ₄₀ N ₃ -COF	2.36	Pt	EtOH	56	-	2
TpPa-2	2.07	Pt	Sodium ascorbate	72.09	-	6
BE-COF	2.12	Pt	Ascorbic acid	76.0	-	7
TFA-COF	2.40	Pt	TEOA	80	-	3
PTP-COF	2.1	Pt	TEOA	83.83	-	8
N ₁ -COF	2.6-2.7	Pt	TEOA	90	0.077 (450 nm) ^c	4
N ₁ -COF	-	Co-1	TEOA	100	-	9
CTP-1	2.96	Pt	TEOA	120	-	10
sp ² c-CMP	1.96	Pt	TEOA	140	-	11
TTR-COF	2.71	Au	TEOA	141	-	12
TTB-COF	2.8	Au	TEOA	145.25	-	12
N ₃ -COF	-	Co-1	TEOA	163	-	9
OB-POP-1	2.21	Pt	TEOA	168	-	13
CTF-1	2.23	Pt	TEOA	168	-	14
B-CTF-1	2.14	Pt	TEOA	179	-	14
TpPa-COF-NO ₂	1.92	Pt	Sodium ascorbate	220	-	15
COF-42	-	Co-1	TEOA	233	-	9
TP-BDDA	2.31	Pt	TEOA	324 ± 10	1.8 (520 nm) ^d	16
CTF-15	2.58	Pt	TEA	352	15.9 (420 nm) ^e	17
TBC-COF	-	Pt	TEOA	360	0.87 (420 nm) ^d	14
N ₂ -COF	-	Co-2 ^b	TEOA	414	-	9
PyTA-BC-Ph	2.67		ascorbic acid	417	1.83(420nm)	18
N ₂ -COF	2.6-2.7	Pt	TEOA	438	0.19 (450 nm) ^c	4
CTP ₃₀₀	2.36	Pt	TEOA	500	2.4 (405 nm)	10
BtCOF150	2.10	Pt	TEOA	750±25	0.2(420nm)	19
N ₂ -COF	-	Co-1 ^a	TEOA	782	0.16 ^d	9
OB-POP-2	2.28	Pt	TEOA	940	-	13
TpDTz COF	2.07	NiME	TEOA	941	0.2 (400 nm) ^d	20
CTF-1-10min	2.26	Pt	TEOA	1072	9.2 (450 nm) ^d	21

CTF-Th	2.38	Pt	TEOA	1100	-	22
OB-POP-4	2.37	Pt	TEOA	1114	-	13
PyTA-BC	2.71		ascorbic acid	1183	1.46(420nm)	18
TpPa-1-COF	2.02	Pt	Sodium ascorbate	1223	-	23
OB-POP-3	2.14	Pt	TEOA	1322	2.0 (420 nm)	13
sp ² c-COF	1.9	Pt	TEOA	1360	-	11
CTF-O	2.67	Pt	TEOA	1440	2.10 (420 nm)	24
CTF-HUST-1	2.03	Pt	TEOA	1540	-	25
TpPa-COF	2.09	Pt	Sodium ascorbate	1560	-	15
TP-COF	2.28	Pt	Ascorbic acid	1600 (± 80)	-	26
N ₃ -COF	2.6-2.7	Pt	TEOA	1703	0.44 (450 nm) ^c	4
CTF-BT	2.51	Pt	TEOA	1800	-	22
Ni(OH) ₂ ⁻ 2.5%/TpPa-2	-	Ni(OH) ₂	Sodium ascorbate	1895.99	-	6
TFPT-COF	2.8	Pt	TEOA	1970	2.2 (400 nm) ^f	27
CTFS ₁₀	1.87	Pt	TEOA	2000	-	28
PyTz-COF	2.20	Pt	Ascorbic acid	2072.4		29
sp ² c-COF _{ERDN}	1.85	Pt	TEOA	2120	0.48 (495 nm)	11
g-C ₅₄ N ₆ -COF	2.03	Pt	TEOA	2518.9		30
g-C ₄₀ N ₃ -COF	2.36	Pt	TEOA	2596	4.84(± 0.27) (420 nm)	2
Py-FTP-BT- COF	2.34	Pt	Ascorbic acid	2875		31
TpPa-COF- CH ₃	2.10	Pt	Sodium ascorbate	3070	-	15
α -Fe ₂ O ₃ /TpPa- 2-COF (3 : 7)	2.07	Pt	sodium ascorbate	3770	0.137(450nm)	32
CdS- COF(90:10)	-	Pt	Lactic acid	3678	4.2 (420 nm)	5
S-COF	2.10	Pt	Ascorbic acid	4440 (± 140)	-	26
CTF-S	2.47	Pt	TEOA	5320	4.11 (420 nm)	24
TpPa-1	2.11	Pt	Ascorbic acid	5479	-	33
MoS ₂ ⁻ 3%/TpPa-1- COF	2.14	MoS ₂	Ascorbic acid	5585	0.76 (420 nm) ^d	33
CTF-HS _{0.75} -1	2.70	Pt	TEOA	6040	4.2 (420 nm)	25
CTF-BT/Th-1	2.51	Pt	TEOA	6606	7.3(420 nm) ^d	22
CTF-HS _{0.75} -2	-	Pt	TEOA	7100	6.8 (420 nm)	25
TpPa-COF- (CH ₃) ₂	2.06	Pt	Sodium ascorbate	8330	-	15
TP-COF	1.97	PVP-Pt	Ascorbic acid	8420	0.4 (475 nm) ^d	7
Py-ClTP-BT- COF	2.36	Pt	Ascorbic acid	8875	8.45(420nm)	31
CTF-CBZ	2.17	Pt	TEOA	9920	4.07 (420 nm)	34

CN-COF	2.09	Pt	TEOA	10100	20.7 (425 nm) ^d	35
Pd ⁰ /TpPa-1-EosinY	-	-	TEOA	10400	-	36
CTF-N	2.17	Pt	TEOA	10760	4.07 (420 nm)	24
TiO ₂ -TpPa-1-COF (1:3)	2.15	Pt	sodium ascorbate	11190	7.6(420nm)	37
20%CdS-CTF-1	-	Pt	Lactic acid	11430	16.3 (420 nm)	38
CdS NPs/3%CTF-1	2.36	Pt	Lactic acid	12150	-	39
Mo ₃ S ₁₃ @EB-COF	-	Ru(bpy) ₃ C _{l₂}	Ascorbic acid	13215	4.49 (475 nm) ^d	40
ter-CTF-0.7	2.11	Pt	TEOA	19320	22.8 (420 nm)	34
NH ₂ -UiO-66/TpPa-1-COF(4:6)	2.10	Pt	Sodium ascorbate	23413	-	23
FS-COF rGO(5%)–TpPa-1-COF	1.85	Pt	Ascorbic acid	10100 (\pm 300)	3.2 (600 nm) ^e	26
FS-COF+WS5F	2.06	Pt	sodium ascorbate	11980	7.53(450nm)	41
Cu-salphen-HDCOF-NSs+FS	-	Pt	Ascorbic acid	16300 (\pm 290)	2.2 (600 nm) ^e	26
	1.62		TEA	36990	5.77(420 nm)	42

^aCo-1: [Co(dmgH)₂pyCl]; ^bCo-2: [Co(dmgBF₂)₂(OH₂)₂]; ^cPE:Photonic efficiency; ^dAQE: apparent quantum efficiency; ^eEQE: external quantum efficiency; ^fQE: quantum efficiency; TEOA: Triethanolamine; TEA: Triethylamine.

Reference

1. L. Bian, J. Hai, E. Zhu, J. Yu, Y. Liu, J. Zhou, G. Ge and W. Tang, *J. Mater. Chem. A*, 2015, **3**, 1920-1924.
2. S. Bi, C. Yang, W. Zhang, J. Xu, L. Liu, D. Wu, X. Wang, Y. Han, Q. Liang and F. Zhang, *Nat. Commun.*, 2019, **10**, 2467.
3. C. Liu, Y. Xiao, Q. Yang, Y. Wang, R. Lu, Y. Chen, C. Wang and H. Yan, *Appl. Surf. Sci.*, 2021, **537**.
4. V. S. Vyas, F. Haase, L. Stegbauer, G. Savasci, F. Podjaski, C. Ochsenfeld and B. V. Lotsch, *Nat. Commun.*, 2015, **6**, 8508.
5. J. Thote, H. B. Aiyappa, A. Deshpande, D. Díaz Díaz, S. Kurungot and R. Banerjee, *Chem. Eur. J.*, 2014, **20**, 15961-15965.
6. H. Dong, X.-B. Meng, X. Zhang, H.-L. Tang, J.-W. Liu, J.-H. Wang, J.-Z. Wei, F.-M. Zhang, L.-L. Bai and X.-J. Sun, *Chem. Eng. J.*, 2020, **379**, 122342.
7. J. Ming, A. Liu, J. Zhao, P. Zhang, H. Huang, H. Lin, Z. Xu, X. Zhang, X. Wang, J. Hofkens, M. B. J. Roeffaers and J. Long, *Angew. Chem. Int. Ed.*, 2019, **58**, 18290-18294.
8. F. Haase, T. Banerjee, G. Savasci, C. Ochsenfeld and B. V. Lotsch, *Faraday Discuss.*, 2017, **201**, 247-264.

9. T. Banerjee, F. Haase, G. Savasci, K. Gottschling, C. Ochsenfeld and B. V. Lotsch, *J. Am. Chem. Soc.*, 2017, **139**, 16228-16234.
10. Z.-A. Lan, Y. Fang, X. Chen and X. Wang, *Chem. Commun.*, 2019, **55**, 7756-7759.
11. E. Jin, Z. Lan, Q. Jiang, K. Geng, G. Li, X. Wang and D. Jiang, *Chem.*, 2019, **5**, 1632-1647.
12. L. Y. Li, Z. M. Zhou, L. Y. Li, Z. Y. Zhuang, J. H. Bi, J. H. Chen, Y. Yu and J. G. Yu, *ACS Sustain. Chem. Eng.*, 2019, **7**, 18574-18581.
13. S. Bi, Z.-A. Lan, S. Paasch, W. Zhang, Y. He, C. Zhang, F. Liu, D. Wu, X. Zhuang, E. Brunner, X. Wang and F. Zhang, *Adv. Funct. Mater.*, 2017, **27**, 1703146.
14. F. Li, D. Wang, Q.-J. Xing, G. Zhou, S.-S. Liu, Y. Li, L.-L. Zheng, P. Ye and J.-P. Zou, *Appl. Catal. B: Environ.*, 2019, **243**, 621-628.
15. J.-L. Sheng, H. Dong, X.-B. Meng, H.-L. Tang, Y.-H. Yao, D.-Q. Liu, L.-L. Bai, F.-M. Zhang, J.-Z. Wei and X.-J. Sun, *ChemCatChem*, 2019, **11**, 2313-2319.
16. P. Pachfule, A. Acharjya, J. Roeser, T. Langenhahn, M. Schwarze, R. Schomäcker, A. Thomas and J. Schmidt, *J. Am. Chem. Soc.*, 2018, **140**, 1423-1427.
17. C. B. Meier, R. Clowes, E. Berardo, K. E. Jelfs, M. A. Zwijnenburg, R. S. Sprick and A. I. Cooper, *Chem. Mater.*, 2019, **31**, 8830-8838.
18. A. F. M. El-Mahdy, A. M. Elewa, S.-W. Huang, H.-H. Chou and S.-W. Kuo, *Adv. Opt. Mater.*, 2020, **8**.
19. S. Ghosh, A. Nakada, M. A. Springer, T. Kawaguchi, K. Suzuki, H. Kaji, I. Baburin, A. Kuc, T. Heine, H. Suzuki, R. Abe and S. Seki, *J. Am. Chem. Soc.*, 2020, **142**, 9752-9762.
20. B. P. Biswal, H. A. Vignolo-González, T. Banerjee, L. Grunenberg, G. Savasci, K. Gottschling, J. Nuss, C. Ochsenfeld and B. V. Lotsch, *J. Am. Chem. Soc.*, 2019, **141**, 11082-11092.
21. S. Kuecken, A. Acharjya, L. Zhi, M. Schwarze, R. Schomäcker and A. Thomas, *Chem. Commun.*, 2017, **53**, 5854-5857.
22. W. Huang, Q. He, Y. Hu and Y. Li, *Angew. Chem. Int. Ed.*, 2019, **58**, 8676-8680.
23. F.-M. Zhang, J.-L. Sheng, Z.-D. Yang, X.-J. Sun, H.-L. Tang, M. Lu, H. Dong, F.-C. Shen, J. Liu and Y.-Q. Lan, *Angew. Chem. Int. Ed.*, 2018, **57**, 12106-12110.
24. L. Guo, Y. Niu, H. Xu, Q. Li, S. Razzaque, Q. Huang, S. Jin and B. Tan, *J. Mater. Chem. A*, 2018, **6**, 19775-19781.
25. N. Wang, G. Cheng, L. Guo, B. Tan and S. Jin, *Adv. Funct. Mater.*, 2019, **0**, 1904781.
26. X. Wang, L. Chen, S. Y. Chong, M. A. Little, Y. Wu, W.-H. Zhu, R. Clowes, Y. Yan, M. A. Zwijnenburg, R. S. Sprick and A. I. Cooper, *Nat. Chem.*, 2018, **10**, 1180-1189.
27. L. Stegbauer, K. Schwinghammer and B. V. Lotsch, *Chem. Sci.*, 2014, **5**, 2789-2793.
28. L. Li, W. Fang, P. Zhang, J. Bi, Y. He, J. Wang and W. Su, *J. Mater. Chem. A*, 2016, **4**, 12402-12406.
29. W. Li, X. Huang, T. Zeng, Y. A. Liu, W. Hu, H. Yang, Y.-B. Zhang and K. Wen, *Angew. Chem. Int. Ed.*, 2020, **60**, 1869-1874.
30. J. Xu, C. Yang, S. Bi, W. Wang, Y. He, D. Wu, Q. Liang, X. Wang and F. Zhang, *Angew. Chem. Int. Ed.*, 2020, **59**, 23845-23853.
31. W. Chen, L. Wang, D. Mo, F. He, Z. Wen, X. Wu, H. Xu and L. Chen, *Angew. Chem. Int. Ed.*, 2020, **59**, 16902-16909.
32. Y.-P. Zhang, H.-L. Tang, H. Dong, M.-Y. Gao, C.-C. Li, X.-J. Sun, J.-Z. Wei, Y. Qu, Z.-J. Li and F.-M. Zhang, *J. Mater. Chem. A*, 2020, **8**, 4334-4340.

33. M. Y. Gao, C. C. Li, H. L. Tang, X. J. Sun, H. Dong and F. M. Zhang, *J. Mater. Chem. A*, 2019, **7**, 20193-20200.
34. L. Guo, Y. Niu, S. Razzaque, B. Tan and S. Jin, *ACS Catal.*, 2019, **9**, 9438-9445.
35. M. Luo, Q. Yang, K. Liu, H. Cao and H. Yan, *Chem. Commun.*, 2019, **55**, 5829-5832.
36. S.-Y. Ding, P.-L. Wang, G.-L. Yin, X. Zhang and G. Lu, *Int. J. Hydrogen Energ.*, 2019, **44**, 11872-11876.
37. C.-C. Li, M.-Y. Gao, X.-J. Sun, H.-L. Tang, H. Dong and F.-M. Zhang, *Appl. Catal. B: Environ.*, 2020, **266**.
38. D. Wang, H. Zeng, X. Xiong, M.-F. Wu, M. Xia, M. Xie, J.-P. Zou and S.-L. Luo, *Sci. Bull.*, 2020, **65**, 113-122.
39. D. Wang, X. Li, L.-L. Zheng, L.-M. Qin, S. Li, P. Ye, Y. Li and J.-P. Zou, *Nanoscale*, 2018, **10**, 19509-19516.
40. Y.-J. Cheng, R. Wang, S. Wang, X.-J. Xi, L.-F. Ma and S.-Q. Zang, *Chem. Commun.*, 2018, **54**, 13563-13566.
41. Y.-H. Yao, J. Li, H. Zhang, H.-L. Tang, L. Fang, G.-D. Niu, X.-J. Sun and F.-M. Zhang, *J. Mater. Chem. A*, 2020, **8**, 8949-8956.
42. Y. Zang, R. Wang, P.-P. Shao, X. Feng, S. Wang, S.-Q. Zang and T. C. W. Mak, *J. Mater. Chem. A*, 2020, **8**, 25094-25100.